13th World Conference on Earthquake Engineering
Vancouver, B.C., Canada
August 1-6, 2004
Paper No. 7009

FRACTURE MECHANICS BASED BENDING FAILURE ANALYSIS FOR FIBER REINFORCED LIGHT-WEIGHT CONCRETE PANEL CONSIDERING CRACK DISPERSION EFFECT

Yoshinori KITSUTAKA [1]

SUMMARY

In this study, the fracture process of strain softening and hardening material which has the crack dispersion and localization characteristics was studied. Numerical analysis method to calculate the load displacement relationship of the member which has multiple cracking subjected to the bending was proposed based on the fracture mechanics consideration. Bending tests of the fiber reinforced light-weight concrete panel were performed. Influences of the fiber content and the air content on the mechanical properties and on the crack dispersing effect were cleared. Especially, the fiber reinforced light-weight concrete containing air showed high crack dispersion under the bending condition. Tension softening diagram of fiber reinforced light-weight concrete which can be used as a constitutive law for the numerical analysis were evaluated by the data of a load - crack mouth opening displacement (CMOD) relationships obtained by the wedge splitting test. The analysis results of the bending tests agreed well with the test results.

INTRODUCTION

Active research has been conducted in recent years regarding subjects related to the high performance of concrete materials. Among such subjects, enhancement of the ductility of concrete by fiber reinforcement is of paramount importance from the aspect of improving the safety performance and durability of concrete members, as high ductility increases the energy absorption of concrete during its failure process. The failure of fiber-reinforced concrete is characterized by being more ductile than that of conventional concrete, thanks to bridging of fibers, which continues to transfer the tensile stress after cracking. The transferred stress may even increase after cracking, which is known as strain hardening. In such a state, partial hardening in the failure process of a member causes new cracks in other parts of the member, dispersing the fracture process zones. This increases the energy-absorbing capacity of the member during failure, while avoiding brittleness due to localization of cracking, thereby leading to an ideal mode of failure. Such behavior of fiber-reinforced materials during failure in tension can be experimentally and analytically evaluated as tension softening properties [1], and such properties have been reported in regard to a wide variety of fiber reinforced concretes [2]. Fundamental studies on the stress-transfer mechanism of fiber-reinforced materials have also been reported [3,4]. Nevertheless, these mostly refer to evaluation

[1] Professor, Tokyo Metropolitan University, Tokyo, Japan. Email: kitsu@comp.metro-u.ac.jp

on the element level with a limited fracture process zone, and few studies have modeled the crack dispersion found in the failure of actual members. Modeling of the process of dispersion/localization of fracture process zones is crucial, particularly for numerical analysis of the load-deformation relationship of members.

Other applications of fiber-reinforced concrete include pre-cast concrete members for buildings, curtain-walls, and panel materials, for which weight reduction is desired from the aspect of seismic safety.

This paper reports on an investigation into the failure of composite materials exhibiting softening and hardening phenomena and presents a simple model of failure dispersion/localization. An analysis method for load-deformation relationship on the member level is proposed as well. The bending failure properties of fiber-reinforced lightweight concrete panels are also investigated, with the validity of the proposed analysis method for load-deformation relationship being examined.

ANALYSIS METHOD

Models and analysis method for dispersion/localization of failure

Figure 1 shows typical failure processes when nonlinear elements, El_1 and El_2, made of the same material (e.g., fiber-reinforced material) having initial defects of different degrees are serially arranged and undergo tension softening and hardening. As the load increases, cracking gradually occurs in each element (*a*, *a*'). El_2 having a larger initial defect, in which cracking proceeds in advance of that in El_1, begins to gradually soften after the peak load (Q_b), with the load-transferring capacity between the elements reducing (Q_b to Q_c). This puts El_1 to an unloading path (*b* to *c*). Due to the plastic deformation, El_1 does not fully return to point *a*. If El_2 continues to soften, then failure is localized and intensely proceeds in El_2 (*d*'), while cracking in El_1 begins to close (*d*). Normal softening materials, such as concrete, shows such localization of failure to rupture. However, if El_2 shows a hardening phenomenon from *c*' (*c*' to *e*'), then El_1 enters a re-loading phase (*c* to *b*). The failure of El_1 begins to proceed again after the load exceeds Q_b (*b* to *e*), causing re-dispersion of the fracture process zones. When the load increases further, with El_1 passing the peak load (Q_e), then El_1 begins to soften (*e* to *f*), putting El_2 to an unloading path (*e*' to *f*'). The failure of each element continuously proceeds through these complicated paths, eventually absorbing great energy.

Also, the changes in the tension-softening diagram in the unloading process shown as *b* to *c* in Fig. 1 (apparent relationship between the crack mouth opening displacement (CMOD) and cohesive stress) can be explained as shown in Fig. 2. When the load decreases from Q_b to Q_c, the cohesive stress, σ, decreases uniformly and linearly corresponding to the unloading ratio, $\alpha = Q_c/Q_b$, to σ' (Eq. (1)), assuming that cracking closes from the tip at a constant rate. The CMOD, δ, can be expressed as Eq. (2) by incorporating the plasticity index, *p*, into a. The plasticity index, *p*, expresses the degree of crack closing when unloaded. $p = 0$ when the CMOD is origin-oriented, whereas $p = 1$ when the CMOD remains unchanged after unloading, showing perfect plasticity. During re-loading, the plot returns along the unloading path to the point where unloading began, from which it follows a normal tension–softening diagram (see Fig. 2).

$$\sigma' = \alpha\sigma \tag{1}$$

$$\delta = (\alpha + (1-\alpha)p)\delta \tag{2}$$

The CMOD, Eqs. (1) and (2) allow determination of the CMOD distribution after unloading and calculation of the deformation of the elements. The load-deformation relationship of the entire member is determined by calculating the deformation of each element and superposing all, while assuming that cross

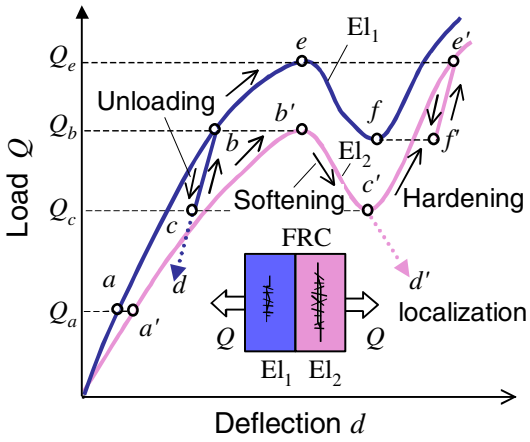

Fig.1 Load-deflection relationship of two hardening elements

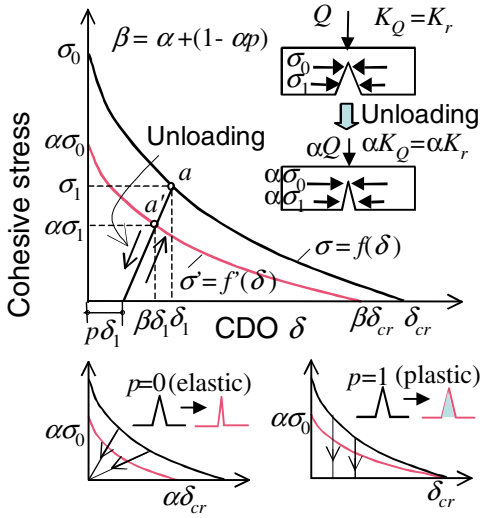

Fig.2 Unloading/reloading model of tension softening diagram

sections remain plane and normal after deformation in the stress transfer between elements (Navier's hypothesis). This analysis flow is shown in Fig. 3.

Analysis method for pure bending failure

Fracture of an element of the pure bending member is modeled for the cohesive force model as shown in Fig. 4. The boundary conditions of the cracked element with cohesive forces are provided by the equilibrium of stress intensity factor and the equilibrium of COD.

$$K_{IM}(a) + K_{Ir}(a) = 0 \tag{3}$$

$$\delta(a,x) = \delta_M(a,x) + \delta_r(a,x) \tag{4}$$

Where a is the crack length, x is the point on the crack surface, $K_{IM}(a)$, $K_{Ir}(a)$ are the mode I stress intensity factors on the crack tip due to the external moment and the cohesive stress, respectively, $\delta(a, x)$ is the COD at x and $\delta_M(a, x)$, $\delta_r(a, x)$ are the CODs due to the external moment and the cohesive stress, respectively. These relationships can be calculated by using FEM or BEM, but in the case of a simple beam, the solution can be obtained using the calculation results of linear fracture mechanics [5]. $K_{IM}(a)$, $K_{Ir}(a)$ appeared in Eq. (3) are follows.

$$K_{IM}(a) = 6M / d^2 \sqrt{\pi a} \cdot F(a,d) = M \cdot k_M(a) \tag{5}$$

$$K_{Ir}(a) = \int_0^a \frac{2\sigma(a,c)}{\sqrt{\pi a}} \cdot G(a,c,d)\,dc = \int_0^a \sigma(a,c) \cdot k_r(a,c)\,dc \tag{6}$$

M is the nominal moment due to the external load, d is the height of beam, c is the coordinate indicating the point on crack surface where cohesive force is acting (see Fig.4), and $F(a, d)$ and $G(a, c, d)$ are weight functions. For the calculation of COD, Castigliano's theorem is employed. Displacement of cracked body can be expressed by stress intensity factors (K-superposition method) [5];

$$dy = d_0 + \int_x^a \frac{2 \cdot K(z)}{E} \left[\frac{\partial K_f(z)}{\partial f} \right]_{f=0} dz \tag{7}$$

Where dy is the displacement on x, d_0 is the displacement of uncracked body, z is the coordinate indicating the crack length for the integration, f is the fictitious force acting on the point x, E is the elastic modulus, $K(z)$ is the stress intensity factor producing the displacement dy, and $K_f(z)$ is the stress intensity factor due to fictitious force f acting for the direction of dy. Substituting Eqs. (5) and (6) into Eq. (7) and calculating the left hand side of Eq. (4).

$$\delta_M(a,x) = 24M/d^2 \int_x^a \frac{1}{E} F(z,d)\cdot G(z,x,d)dz = M\cdot d_M(a,x) \tag{8}$$

$$\delta_r(a,x) = \int_0^a \sigma(a,c)\left[\frac{8}{\pi}\int_x^a \frac{1}{z\cdot E} G(z,x,d)\cdot G(z,c,d)dz\right]dc = \int_0^a \sigma(a,c)\cdot d_r(a,x,c)dc \tag{9}$$

Substituting Eqs. (5) and (6) to Eq. (3), also Eqs. (8) and (9) to Eq. (4), and canceling the M appeared in Eqs. (3) and (4), then the simple crack integral equation is obtained as Eq. (10). $H(a, x, c)$ is the weight function called the H-function, and it does not depend on the loading condition.

$$\delta(a,x) = \int_0^a \sigma(a,c)\cdot H(a,x,c)d \quad ;H(a,x,c) = k_r(a,c)\cdot d_M(a,x)/k_M(a) - d_r(a,x,c) \tag{10}$$

Tension softening diagram as a constitutive law of material is expressed as Eq. (11). The cohesive stress $\sigma(a, x)$ is the poly-linear function of crack opening displacement (COD) of $\delta(a, x)$.

$$\sigma(a,x) = m(\delta,x)\cdot\delta + n(\delta,x); \quad \delta = \delta(a,x) \tag{11}$$

Where $m(\delta)$ is the softening inclination and $n(\delta)$ is the inflection point. Substituting $\sigma(a, x)$ of Eq. (11) into Eq. (10) and expressing in the matrix form for the total number of nodes (=n) on the crack surface, we obtain the simultaneous crack equation on $\delta(a, x)$. From the solution of the equation, distribution of COD and cohesive stress in the case of crack length a are obtained. Substituting $\sigma(a, x)$ into Eq. (6) and calculating $K_{IM}(a)$ by Eq. (3) then external moment M is obtained by Eq. (5).

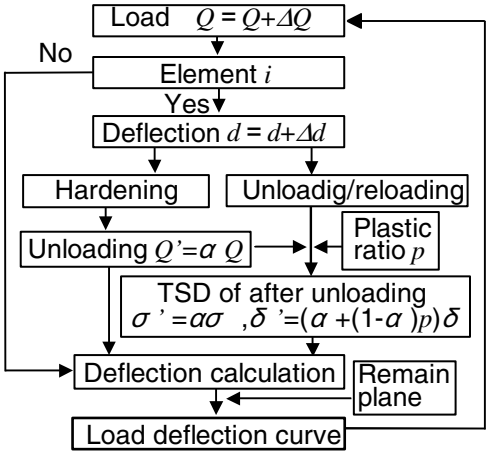

Fig.3 Analysis flow considering unloading/reloading

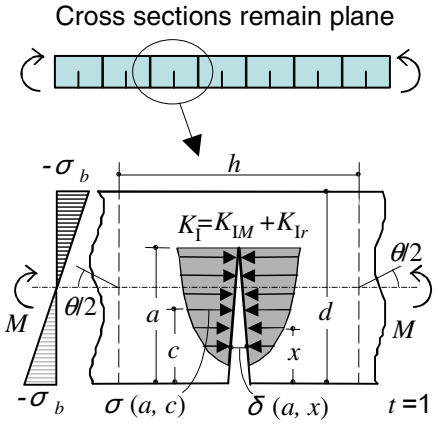

Fig.4 Cohesive force model of bending element for mode I failure

Rotational angle $\theta(a)$ of the element is obtained from the accumulation of the rotational angle due to the external moment and the rotational angle due to the cohesive stress.

$$\theta(a) = \theta_M(a) + \theta_r(a) \tag{12}$$

The rotational angle θ is expressed as below by using the Castigliano's theorem.

$$\theta = \frac{\partial U_{NoCrack}}{\partial M} + \frac{2}{E}\int_0^a K_{\mathrm{I}} \frac{\partial K_{\mathrm{I}M}}{\partial M} da \tag{13}$$

Substituting Eqs. (5) and (6) into Eq. (13).

$$\theta_M(a) = \theta_{M\,NoCrack} + \frac{2}{E}\int_0^a K_{\mathrm{I}M}(z) \frac{\partial K_{\mathrm{I}M}(z)}{\partial M} dz = \frac{Mh}{EI} + \frac{72\pi M}{Ed^4}\int_0^a z \cdot F(z,d)^2 dz \tag{14}$$

$$\theta_r(a) = \left(\theta_{M\,NoCrack}\right)_{M=0} + \frac{2}{E}\int_x^a K_{\mathrm{I}r}(z)\left[\frac{\partial K_{\mathrm{I}M}(z)}{\partial M}\right]_{M=0} dz = \frac{24}{Ed^2}\int_0^a \sigma(a,c)\left[\int_0^a F(z,d)\cdot G(z,c,d)dz\right]dc \tag{15}$$

In $\theta_r(a)$, considering the moment M as fictitious moment as M=0. Substituting Eqs. (14) and (15) into Eq. (12), then relation of M and $\theta(a)$is obtained. From the result of rotational angle, curvature $k=\theta/h$ of each element is calculated, and total deflection of the beam is calculated by assuming cross sections remain plane.

TEST PROCEDURES

Specimens

Table 1 gives the materials used in the tests. In consideration of the application to pre-cast concrete members, the materials comprised high-early-strength portland cement, foamed artificial lightweight aggregate made from waste glass, and an air-entraining and high-range water-reducing admixture and an air foaming agent as the cement, fine aggregate, and chemical admixtures, respectively. Vinylon fibers, which were found effective in improving the ductility and reducing the weight of concrete, were used as short fibers. These were proportioned with a water-binder ratio (W/B) of 20%. Normal strength concrete specimens were also fabricated for reference.

Table 1 Materials used

Symbol	Materials	Properties
C	Cement	high-early-strength portland cement, ρ = 3.15
SF	Silica fume	SiO_2 96.8%, ρ = 2.20
VF	Vinylon fiber (RF4000)	ρ = 1.30, length=30mm, diameter=660(μ m), tensile strength=900(MPa), Young's modulus=30(GPa)
GL	Waste glass aggregate	#1 : #2 : #3 = 8 : 1 : 1 (weight ratio), maximum size=5mm, ρ = 0.70, water absorption=7%
SP	Super plasticizer	-
AE	AE agent	-
FA	Foaming agent	-
S	Crashed sand	ρ = 2.62
G	Crashed stone	ρ = 2.66

Table 2 gives the proportioning conditions for the specimens. A 70-ml omni mixer was used for mixing. Three cylindrical specimens (ϕ100 × 200 mm) for compression and elastic modulus testing, three prismatic specimens (100 × 100 × 120 mm) for wedge splitting, and two panel specimens (300 × 100 × 900 mm) for panel bending testing were prepared for each mixture. Specimens were demolded at an age of one day and then water-cured at 20°C up to an age of 12 weeks. Table 3 gives the properties of the mixtures while fresh and strength properties of the specimens.

Table 2 Mix proportions

a) plain concrete

Symbol	W/C (%)	Absolute weight(kg/m³)			
		Water	Cement	Fine aggregate	Coarse aggregate
NC	65	180	277	756	1152

b) the other concrete

Symbol	W/B (%)	Foaming agent (B×%)	Absolute weight (kg/m³)							
			Water	Cement	GL	SF	Agent			VF
							SP	Fa	AE	
LP	20	0	121	677	420	75	30.1	—	4.5	
LPa		1.0	113	677		75	30.1	7.5	4.5	
LF		0	118	660		73	29.3	—	4.4	13.0
LFa		1.0	110	660		73	29.3	7.5	4.4	13.0

Table 3 Properties of specimens

Symbol	Slump (cm)	Slump flow (cm×cm)	Specific gravity	Air content (%)	Compressive strength (MPa)	Young's modulus (GPa)
NC	16.5	19×18	2.35	0.66	27.6	29.3
LP	25.5	50×50	1.29	4.73	37.4	14.7
LPa	23.5	39×39	1.04	23.79	17.6	8.6
LF	24.0	47×46	1.29	4.25	41.7	13.3
LFa	24.5	46×46	1.02	24.42	19.6	8.5

Wedge splitting testing

The tension-softening diagram, which is used as the constitutive law in the numerical analysis, was evaluated by wedge splitting testing, whereby mode I failure (tensile deformation) is obtained with small specimens. A notch was cut in the center of each specimen using a diamond cutter with a tooth thickness of 1 mm, leaving a ligament depth of 50 mm, at which tensile failure was induced by inserting a wedge (Fig. 5). A servo-controlled hydraulic tester having a closed loop system (manufactured by MTS) was used to achieve accurate measurement of the load-displacement curves. This testing machine permits control of the displacement rate by adjusting the hydraulic servo valve, while using the clip gauge measurement of the CMOD as the feedback signal. The displacement rates by the CMOD were set at 0.002 mm/min for normal and fiber-reinforced concrete specimens, whereas the rate was set at 0.0005 mm/min for lightweight concrete with no fibers, since this type of concrete tends to lead to brittle failure. Sensitive clip gauges for displacement control (MTS-632.02) were used for the CMOD measurement. The tension-softening diagram was determined by poly-linear approximation analysis method [6] based on the obtained load-CMOD curves.

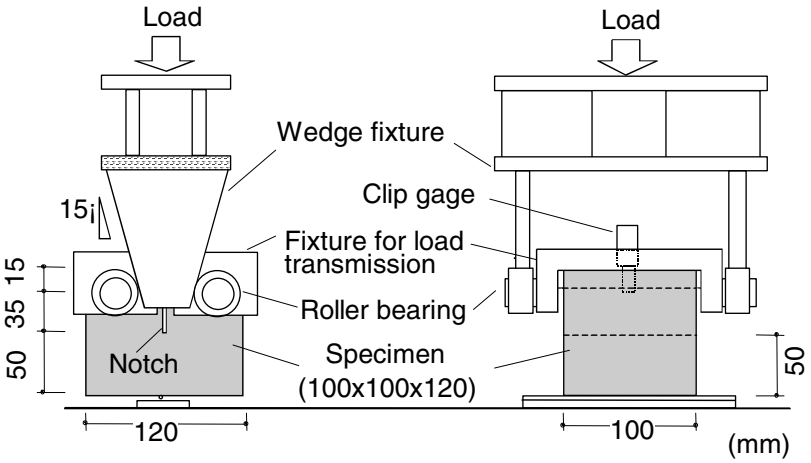

Fig.5 Wedge splitting test

Panel bending testing

Figure 6 shows the schematic of panel bending testing. A 100-tonf Amsler universal testing machine was used for the bending tests by four-point manually operated loading, with the span between the supports and the central span between the loading points being 800 mm and 400 mm, respectively. The midspan deflections at both bottom edges were measured. Seven strain gauges with a gauge length of 60 mm were also glued to the bottom of each specimen to measure the state of cracking and degree of crack dispersion.

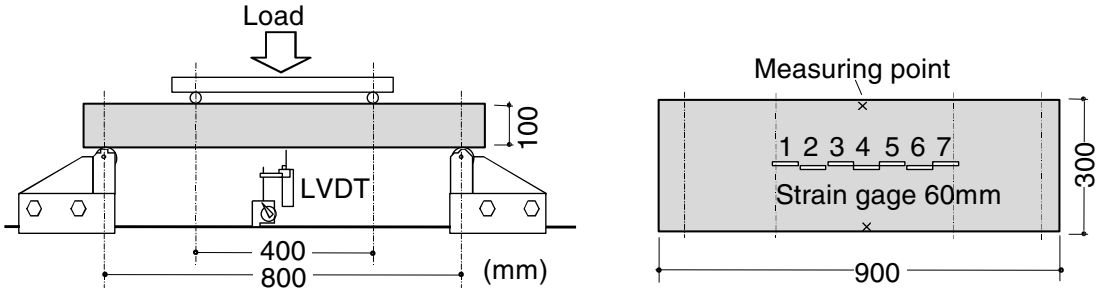

Fig.6 Bending test of panel specimen

TEST RESULTS AND DISCUSSION

Load-CMOD curves

Figure 7 shows the load-CMOD curves obtained from wedge splitting tests by averaging the data for each mixture. Among the specimens with no fibers, LP containing no foaming agent did not achieve stable failure, leading to brittle failure, but LPa containing a foaming agent underwent relatively stable failure, though the strength was lower than that of LP. When compared with normal concrete, NC, the areas under the curves of both LP and LPa are small, indicating their small energy-absorbing capacities. Regarding specimens reinforced with fibers, the peak loads of LF and LFa are similar to those of specimens with no fibers, but subsequent loads are maintained high, indicating substantial improvement in their ductility. It is particularly notable that the loads re-increase after a tentative post-peak drop, indicating the hardening phenomenon. The area under the curve and the peak load of foamed LFa are lower than those of LF with no foams. This may be because the inclusion of foams reduces the strength of the matrix, while reducing the areas of bond between fibers and paste, thereby reducing the load-transferring capacity.

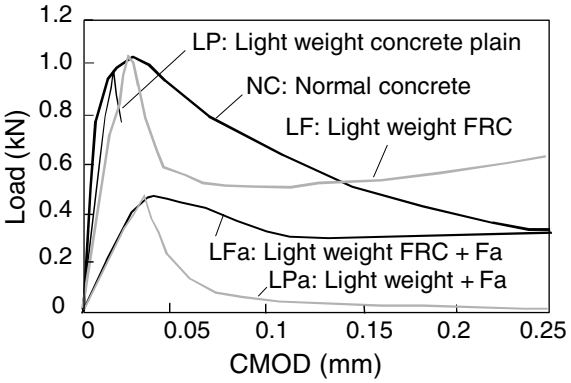

Fig.7 Load ĞCMOD curve (average)

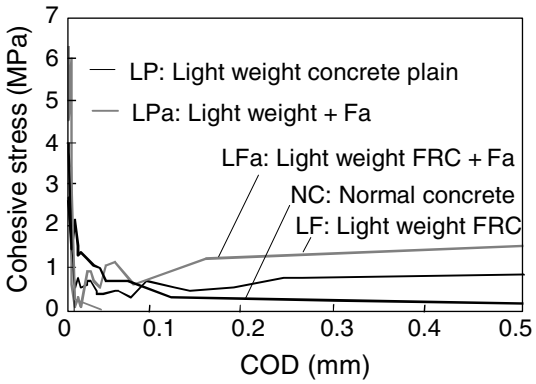

Fig.8 Tension softening diagram

Tension softening diagram

Figure 8 shows the tension-softening diagrams (TSDs) determined by poly-linear approximation. Reflecting the load-CMOD curves, the TSDs of mixtures showing high ductility by the load-CMOD curves show moderate softening with large areas under the lines. The TSDs of specimens with fibers are level or rising toward the right-hand side, indicating the stress transfer despite the increased CMOD. The obtained TSDs were linearly approximated into two to five lines for analysis.

Bending test results of panel specimens

Figure 10 shows the load-deflection curves obtained from the panel bending tests. Though the maximum strengths of specimens containing fibers (LF and LFa) are similar to those of specimens with no fibers, their failure is more ductile, without reaching failure immediately after the maximum loads. The load on LF with no foams tentatively drops after the peak load but gradually recovers. The load on foamed LFa retains a rising tendency after the peak load, showing several subsequent peaks. Observation of the panel crack patterns after the bending tests revealed one large crack in each of NC, LP, and LPa. Among the specimens with fibers, LF showed certain fine dispersion of cracks, whereas LFa showed significant dispersion of cracks in contrast to other specimens.

Changes in strain by panel bending testing

Figure 9 shows the strains measured at the bottom surfaces of panels (one specimen each). On the NC specimen, the strains are uniformly distributed up to a deformation of 0.4 mm, which is before the peak load, but a large strain develops partially when the deformation is 0.5 mm near the peak load, indicating localization of failure. On the LPa specimen with foams, the strains are uniformly distributed up to a deformation of pre-peak 0.4 mm similarly to NC, and large strains develop at two points with a near-peak 0.5 mm deformation, indicating failure dispersion. Among the specimens containing fibers, the strains of LF uniformly increase up to a deformation of near-peak 1.0 mm but concentrate after the peak load, indicating localization of failure. The uniform strains before the peak load are greater than those of LP, which can be attributed to occurrence of finely distributed cracks due to bridging of fibers. LF is also characterized by the reductions in the strains at other points when the strain is concentrated and cracking is localized, indicating substantial unloading at other points. This suggests closing (recovery) of fine cracks. On foamed LFa, the strain has already been distributed to several points by the time when the deformation reaches 1 mm, and the strain remains distributed after the peak load, indicating significant dispersion of failure.

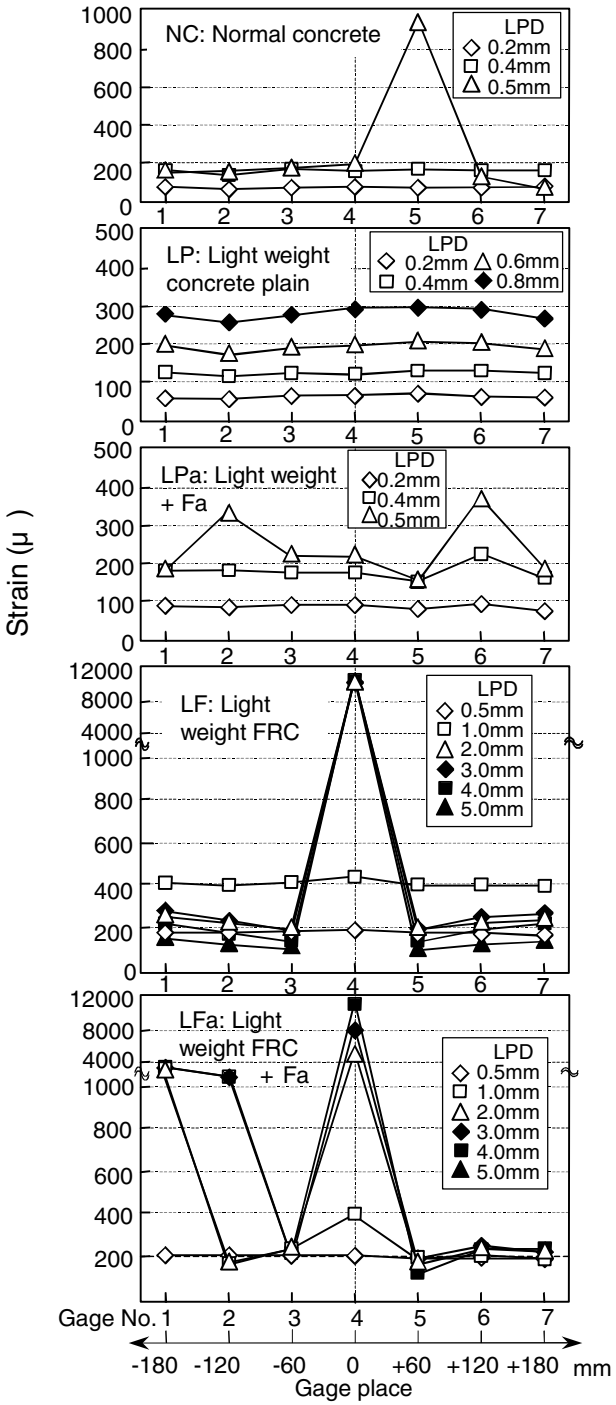

Fig.9 Strains distribution measured at the bottom surfaces of panels

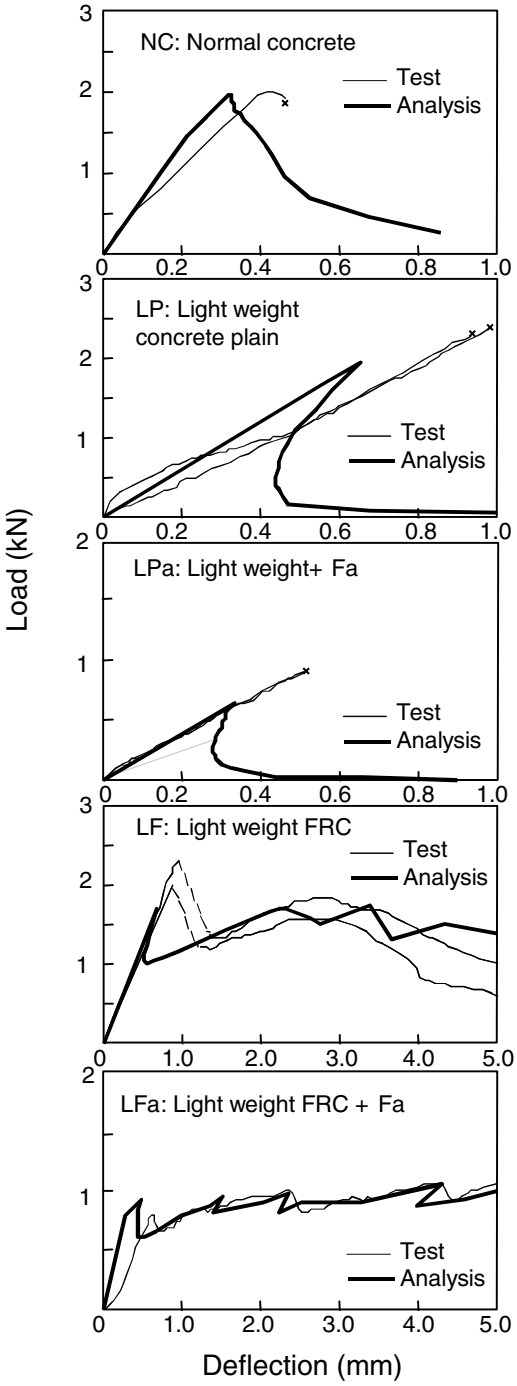

Fig.10 Load-deflection curves obtained from the panel bending tests

RELATIONSHIP BETWEEN ANALYSIS AND TEST RESULTS

Analysis conditions

Bending analysis was conducted by the method proposed in this paper, and the results were compared with the panel bending test results. The geometry of specimens and the loading conditions were the same as those adopted for the tests. The TSD determined by wedge splitting testing for tension and approximated to multiple lines was used as the material constitutive law. Linear elasticity was assumed for the compressive zone. The elastic modulus was determined from the compression test results of cylindrical specimens. As for the width of elements, h, 50 mm was adopted, because analysis conducted with h being set at 50 and 100 mm led to no marked differences among mixtures, and because a width of 50 mm corresponded better to the test results. The 400-mm central span under pure bending were divided into eight elements. The initial defect was modeled by randomly selecting an initial notch with a length of 1 to 5 mm with 1-mm intervals and assuming it at the center of each element. According to the flow shown in Fig. 3, cracking was allowed to develop from the weakest elements having 5-mm initial notches, and the changes in the rotation angle of each element were sequentially determined according to the moment at the time of softening and hardening of the weakest elements. The curvature distribution was then determined from the rotation angles. Regarding this as the loads, the moment diagram was determined to obtain the midspan deflection. The plasticity index p was set at 0.5, as the index values of 0, 0.5, and 1.0 led to no marked differences in the analysis results.

Analysis results and discussion

Figure 11 shows examples of calculation of the moment-rotation angle of each element carried out in the analysis process. In regard to NC, an element having a larger initial notch is found to lead to a smaller peak moment and reach the peak earlier than other elements. The strain-hardening phenomenon of LFa owing to fibers is adequately expressed, in which it tentatively softens but begins to harden on the way, eventually exceeding the primary peak load.

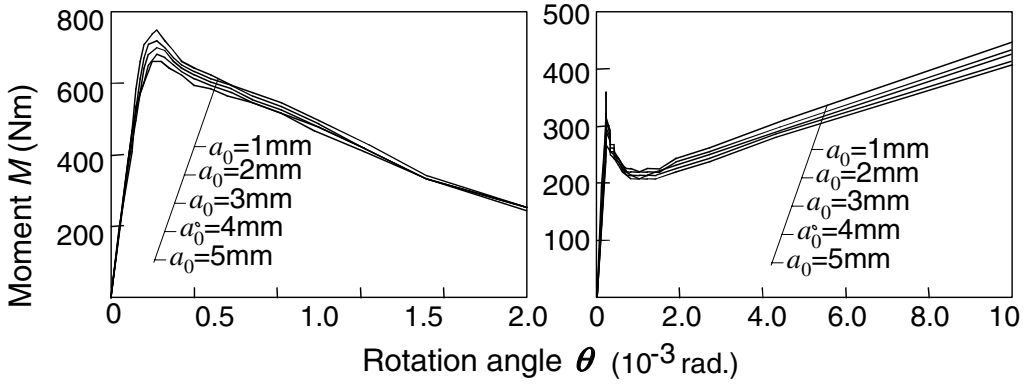

Fig.11 Examples of calculation of the moment-rotation angle of the element

The relationship between the analysis and test results is also shown in Fig. 10. The analysis and test results generally agree well. Though the peak loads for LP and LPa with no fibers are slightly lower than the test results, the load-displacement curves show the snapback phenomenon in which the deformation "turns back" after the peak load, accurately expressing the unstable failure observed in the tests. The test and analysis results of LF and LFa with fibers agree well, particularly well-expressing the deformation capacity after the peak load. The analysis results express the re-loading of at which each element reaches

the peak load being marked with sequential numbers. The upward and downward curves found in the test results of LFa particularly agree well with the analysis results.

CONCLUSIONS

The results obtained in this study are summarized as follows:

(1) The progress of failure involving crack dispersion and localization was modeled with combinations of multiple elements incorporating tension softening. Using this model, an analysis method for load-displacement relationship was proposed, in which unloading and re-loading associated with the softening and hardening of elements are incorporated.

(2) Bending tests on various concrete panels revealed that the inclusion of short fibers disperses the cracks, thereby improving the energy-absorbing capacity of the panels. Crack dispersion was particularly evident in lightweight fiber-reinforced panels containing large amount of foams to reduce the panel weight.

(3) The analyzed load-displacement relationships of various concrete panels under bending nearly agreed with the test results. The deformability of fiber-reinforced materials associated with post-peak softening and hardening was particularly well-expressed by the analysis results.

REFERENCES

1. Li VC, Liang E. “Fracture Processes in Concrete and Fiber Reinforced Cementitious Composites.” Journal of Engineering Mechanics, ASCE; 112(6): 566-586, 1986.
2. Kitsutaka Y, Oh-oka T. “Application of Ultra-light Weight Fiber Reinforced Concrete for the Increased Earthquake Resisting Walls.” 12th World Conference on Earthquake Engineering, Auckland, New Zealand, Paper no. 2470, 2000.
3. Evans AG. “Perspective on the Development of High-toughness Ceramics.” Journal of the American Ceramic Society; 73(2): 187-206, 1990.
4. Li VC, Leung CKY. “Steady-State and Multiple Cracking of Short Random Fiber Composites.” Journal of Engineering Mechanics, ASCE; 118(11): 2246-2264, 1992.
5. Tada H, Paris PC, Irwin GR. “The Stress Analysis of Crack Handbook.” Second Edition: Paris Productions Incorporated, 1985.
6. Kitsutaka Y. ”Fracture Parameters by Poly-linear Tension Softening Analysis.” Journal of Engineering Mechanics, ASCE; 123(5): 444-450, 1997.